PLANETARY SCIENCE

Deep magma storage during the 2021 La Palma eruption

Kyle Dayton[1], Esteban Gazel[1]*, Penny Wieser[2], Valentin R. Troll[3,4,5], Juan Carlos Carracedo[5], Hector La Madrid[6], Diana C. Roman[7], Jamison Ward[8], Meritxell Aulinas[9,10], Harri Geiger[11], Frances M. Deegan[3,4], Guillem Gisbert[9], Francisco J. Perez-Torrado[5]

The 2021 La Palma eruption provided an unpreceded opportunity to test the relationship between earthquake hypocenters and the location of magma reservoirs. We performed density measurements on CO_2-rich fluid inclusions (FIs) hosted in olivine crystals that are highly sensitive to pressure via calibrated Raman spectroscopy. This technique can revolutionize our knowledge of magma storage and transport during an ongoing eruption, given that it can produce precise magma storage depth constraints in near real time with minimal sample preparation. Our FIs have CO_2 recorded densities from 0.73 to 0.98 g/cm^3, translating into depths of 15 to 27 km, which falls within the reported deep seismic zone recording the main melt storage reservoir.

INTRODUCTION

One of the most important challenges in modern volcanology studies is constraining the depth of magmatic reservoirs that supply and sustain eruptions (*1*). However, commonly used methods such as mineral-melt barometry have relatively low precision and accuracy, with standard error estimates of ±200 to 400 MPa (±4 to 7 km) (*2*), which can span the entire crustal column in most ocean-islands or mid-oceanic ridges. These shortcomings have necessitated the use of pre- and syn-eruptive earthquake swarm locations as critical resources to illuminate our understanding of melt migration, but these do not necessarily pinpoint the location of magma storage reservoirs within the lithosphere (*3*–*7*).

The 2021 eruption of Tajogaite on La Palma (Canary Islands, Spain) provides an unpreceded opportunity to study a volcanic magma storage system given the open-source availability of earthquake and ground deformation data paired with near-real-time field sampling campaigns. Here, we performed Raman spectroscopic measurements of fluid inclusions (FIs) in olivine crystals from tephra spanning the length of the eruption using the fact that the densities of CO_2-rich fluids are highly sensitive to pressure, and this relationship is well constrained physically through an equation of state (EOS) (see the Supplementary Materials) (*8*), unlike the empirically calibrated mineral-liquid barometers describing the relatively weak relationship between pressure and mineral composition (*2*, *9*, *10*). While the utility of CO_2 FI has been demonstrated in previous studies of volcanic plumbing systems (*1*, *5*, *11*, *12*) using microthermometry (heating-cooling stage), this study is the first of its kind to use an accurately calibrated Raman technique to constrain the depth of the magma reservoir rapidly and precisely on a time scale relevant to active eruptions. This technique can revolutionize our understanding of magma storage and transport during an ongoing eruption as we collected data on 120 FI in less than a week, including sample preparation, Raman spectroscopy analyses, and data reduction. We demonstrate the enormous potential of this technique as a form of rapid-response petrological monitoring to provide near-real-time information on plumbing system geometry, which can be used in hazard assessment during volcanic crises [e.g., (*13*)].

The island of La Palma in the Canary Islands includes an extinct volcanic complex in the North (Taburiente) and the active Cumbre Vieja Ridge (CVR) in the South (<125 thousand years) (Fig. 1, A and B). The CVR is the most volcanically active region in the Canary Islands (Fig. 1C) (*14*). Along this ridge, eruptive vents align to form a characteristic ocean island rift zone. Most lavas that erupt at the CVR are silica undersaturated basanites and tephrites, but small volumes of evolved phonolites also occur (*11*, *14*). On the basis of the record from eroded rift systems of other islands, these eruptions are fed by a tightly packed dyke swarms within the rifts (*14*, *15*). The intrusion of one such dyke, or possibly a series of dykes, initiated the eruption on the western flank of the CVR on September 19 (*16*, *17*).

The 2021 eruption lasted from September 19 to December 13 and is the most substantial historical eruption on La Palma in terms of its volume (~0.2 km^3), duration (85 days), and degree of destruction, amounting to nearly 1 billion euros in damages (*18*). The event was preceded by deep (15 to 35 km) but low-magnitude seismic activity since 2017 (Fig. 1, D and E) (*19*, *20*), with the eruption itself taking place following a week of intense seismic unrest and ground deformation (*16*). This eruption represents a typical Canarian mafic fissure eruption that included effusive lava emission, lava fountaining, and Strombolian activity in a multi-crater vent complex interrupted by episodic phreatomagmatic pulses (*18*). The eruption opened a series of successive vents (six major

[1]Department of Earth and Atmospheric Sciences, Cornell University, Ithaca, NY 14850, USA. [2]Department of Earth and Planetary Sciences, University of California Berkeley, Berkeley, CA 94720, USA. [3]Department of Earth Sciences, Section for Natural Resources and Sustainable Development, Uppsala University, Uppsala, Sweden. [4]Centre of Natural Hazards and Disaster Science (CNDS), Uppsala University, Uppsala, Sweden. [5]Instituto de Estudios Ambientales y Recursos Naturales (i-UNAT), University of Las Palmas de Gran Canaria (ULPGC), Las Palmas de Gran Canaria, Spain. [6]Department of Geological Sciences, University of Missouri, Columbia, MO 65211, USA. [7]Earth and Planets Laboratory, Carnegie Institution for Science, Washington, DC 20015, USA. [8]Department of Earth and Environmental Sciences, University of Minnesota, Minneapolis, MN 55455, USA. [9]Department of Mineralogia, Petrologia, i Geologia Aplicada, Facultat Ciències de la Terra, Universitat de Barcelona, 08007 Barcelona, Spain. [10]Geomodels Research Institute, University of Barcelona, Marti Franques s/n, 08028 Barcelona, Spain. [11]Institute of Earth and Environmental Sciences, University of Freiburg, 79104 Freiburg im Breisgau, Germany.
*Corresponding author. Email: egazel@cornell.edu

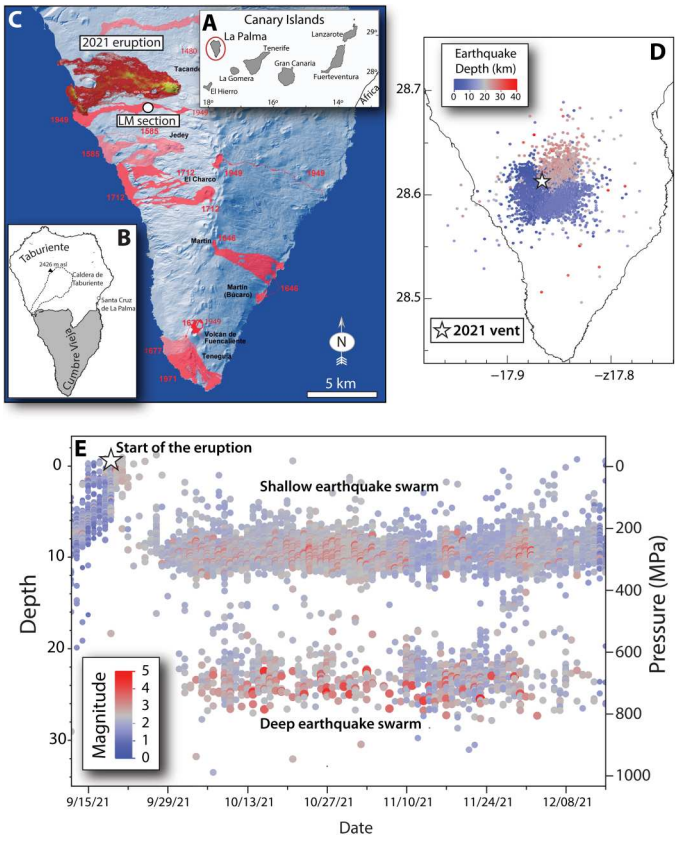

Fig. 1. Seismicity and La Palma 2021. (**A**) Canary Islands. (**B**) Geologic map of La Palma (*18*). (**C**) Details of the historical eruptions of La Palma including the recent 2021 eruption (*18*). (**D**) The 2021 eruption earthquakes colored by depth. (**E**) Earthquake history of the 2021 eruption (*28*). Notice very shallow events just before the beginning (September 9), a bimodal swarm of deep (~20 to 25 km) and shallower (~6 to 12 km) events during the eruption, and a predominately aseismic gap in between. LM denotes the location of the stratigraphic section in the town of Las Manchas.

craters) as it progressed along a >550-m northwest-southeast alignment, ultimately building up a sizable cinder cone (300 m high) and an extensive lava flow field. Throughout the three-month eruption, the intensity of the explosive activity was highly variable, reflected by the variation in seismic intensities and an eruptive column height that was typically around 3500 m above sea level (asl) but reaching up to 8500 m (*21*). Plume height together with emitted pyroclastic volume (~45 million m^3) defines the event as a volcanic explosivity index (VEI) 3, with a total volume (pyroclastic deposits and lava) of >200 million m^3 (Fig. 1C) (*18*).

RESULTS

Tephra samples were collected from a stratigraphic section in the locality of Las Manchas in January 2022 (Fig. 1C and fig. S1). A total of seven layers were defined in the field, which contain the record of the eruption, from September 19 to 21 (LM6) to the end (LM0) (fig. S1). Four samples were selected for FI studies (LM6, LM4, LM2, and LM0). Glass-coated, euhedral olivine crystals (500 μm to 1 mm) were handpicked and cleaned in HBF_4. Individual grains (~200) were mounted and polished for petrographic study and FI identification (fig. S2). We analyzed primary FI (N = 120) (*22*) in 34 olivine crystals (fig. S3) in under a week. These inclusions were analyzed by Raman spectroscopy to determine CO_2 densities based on Fermi diad splitting using the highly accurate and precise calibration method (*23*). All spectroscopy data were collected above the CO_2 critical point (T_{crit} = 31°C) at T = 37°C to ensure homogenization of liquid and vapor into one phase (fig. S4).

Using the CO_2 EOS and an estimate of entrapment temperature (1150°C) (*8*, *24*, *25*), we can relate CO_2 density to pressure (Fig. 2, A to C, and Supplementary Materials). We then convert these pressures into storage depths, assuming a crustal density of ρ = 2.8 g/cm^3 above the Moho (14 km) and ρ = 3.1 g/cm^3 below with the presence of melt (*26*, *27*). All olivine crystals are not in equilibrium with the carrier melt (Fig. 2D), and olivine Mg# varies as the eruption progressed (Fig. 2, D and E). Samples from the early stages of the eruption from September 19 to 21 (LM6) and October (LM4) host FI in relatively evolved olivine crystals (core Mg# 80 to 81%), recording storage depths of 15 to 24 km. Storage depths increase with olivine Mg# (core 84 to 86%) to depths down to 27 km toward the end of the eruption (LM2 and LM0; Fig. 2E). FIs have CO_2 densities ranging from 0.73 to 0.98 g/cm^3, translating to pressures of 420 to 780 MPa and depths of ~15 to 27 km (with most centered around 21 km) below the volcanic center (Fig. 2E).

When compared with the location of earthquake hypocenters during the eruption (Supplementary Materials) (*28*), it is evident that our FIs were trapped/re-equilibrated in the same area as the deep earthquake seismic swarm between ~20 and 25 km (Fig. 3, A and B). These results agree with evidence for deep magma storage in previous CVR eruptions (*29*) and mimic the deep magma plumbing system of the 2014–2015 eruption of Fogo in which FI pressures also align with the seismic data (*5*).

Clinopyroxene-liquid barometry from previous eruptions of the CVR (*25*, *30*–*32*) unsurprisingly span a much wider range of pressures (410 to 1410 MPa) and overlap with the deep seismic zone and the main magma reservoir recorded by our FI densities. The significantly wider spread of clinopyroxene-liquid pressures may reflect the substantially lower precision of mineral melt compared with FI barometry, in addition to the fact that pyroxene crystals may record various depths of crystal growth as opposed to a single magma storage reservoir. The clinopyroxene-liquid barometer (*2*, *9*) used in previous studies has a standard error of ~420 MPa on data not used to calibrate the expression, and analytical errors during analysis of clinopyroxene can easily introduce random error spanning 200 to 600 MPa (Supplementary Materials) (*33*). In contrast, our Monte Carlo simulations show that the 1σ error in calculated pressure resulting from Raman analytical errors (±0.003 g/cm^3) is only ±4.5 MPa (±140 m). When uncertainty in entrapment temperatures (1150° ± 50°C) is also accounted for, the overall errors are still extremely small (1σ = 22 MPa, ~±0.74 km) (Fig. 2E and Supplementary Materials).

DISCUSSION

The depths from our FI densities indicate a level of magma stagnation before the 2021 eruption, but not necessarily the depth of crystallization and FI entrapment. FIs in olivine are susceptible to brittle

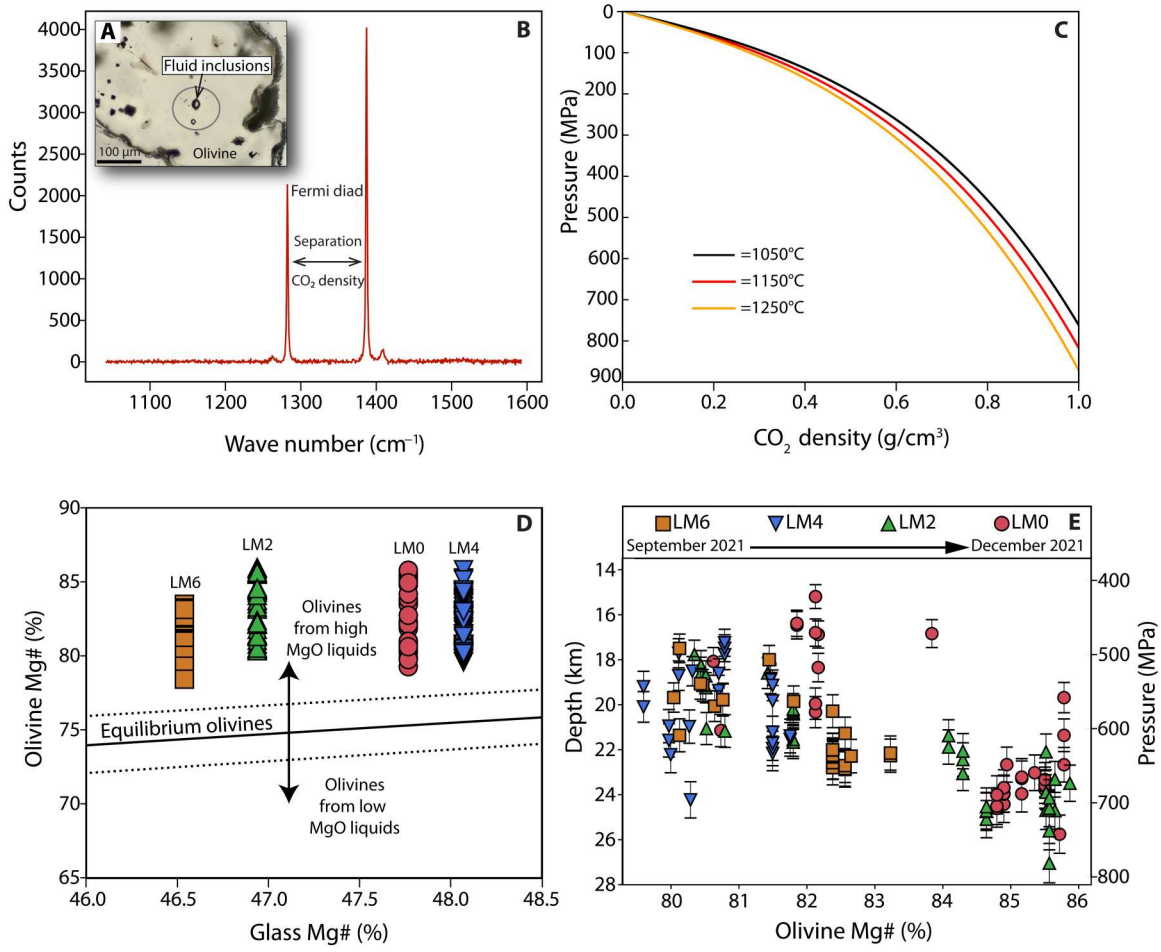

Fig. 2. FI and olivine phenocrysts. (**A**) Example of an olivine-hosted FI from La Palma 2021 eruption. (**B**) CO_2 Raman spectra of the inclusion with a typical Fermi diad split, proportional to the CO_2 density of the inclusion (*8*). (**C**) CO_2 density relation to pressure through the CO_2 EOS. (**D**) Olivine crystals are not in equilibrium with the carrying melt, indicating that the olivine was derived from a higher MgO source (Supplementary Materials). (**E**) FI depths. Notice the increase in FI pressure with crystal Mg# as the eruption proceed. Error bars on FI showing ±1σ from Monte Carlo simulations of uncertainties (Supplementary Materials).

(decrepitation) and plastic (stretching) deformation, which potentially can allow for the modification of trapped CO_2 density (*34*, *35*). Decrepitation results from mechanical failure of the host crystal during ascent due to overpressure of the inclusion within, with larger inclusions more susceptible to rupturing their hosts (*36*). This brittle failure results in cracking of the host crystal and subsequent partial or total loss of fluid held within the inclusions, leading to lower fluid densities (*36*). Inclusions with identifiable decrepitation are present in all analyzed samples, but their densities are not included in this study (fig. S3). Another advantage of this Raman spectroscopy method is the ability to measure small FI (down to 1.5 μm in our samples), which are less susceptible to decrepitation and are too small for the use of microthermometry (*37*).

Unlike decrepitation, which is optically identifiable by a halo of cracks or cylindrical and spherical pores emanating from FI, stretching is a more cryptic phenomenon and is difficult to identify optically. The experiments on originally negative crystal-shaped CO_2-rich FI in San Carlos olivine indicate that FI can stretch at 1400°C and become ellipsoidal on the order of hours (*38*). In addition, when olivine crystals stagnate at high temperature (i.e., in a magma reservoir), re-equilibration of CO_2 density can occur via dislocation creep (*38*). Our measured inclusions are generally ellipsoidal with only weak negative crystal shapes, indicating that FI may have undergone re-equilibration during a period of magma stagnation 15 to 27 km below the CVR before the 2021 eruption (Fig. 3, A and B). This observation aligns with previous studies in the Canary Islands (*1*, *25*, *39*–*43*).

Therefore, it is critical to appreciate that the application of FI barometry to volcanic eruptions is to reveal the final magma staging depth before eruption (*36*), while clinopyroxene barometry may record deeper storage levels feeding the final staging zone. This reservoir may have been replenished multiple times from below, as recorded by the deeper earthquake swarms and potentially illustrated by clinopyroxene barometry from this and previous eruptions (*25*, *30*–*32*, *44*).

Plumbing system of La Palma

The 2021 La Palma eruption shares similarities to historical eruptions along the CVR (*18*, *45*). For instance, the 1949 eruption also emitted early tephritic lavas, which evolved to basanitic compositions in later stages (*29*). Like those found within the basanite of

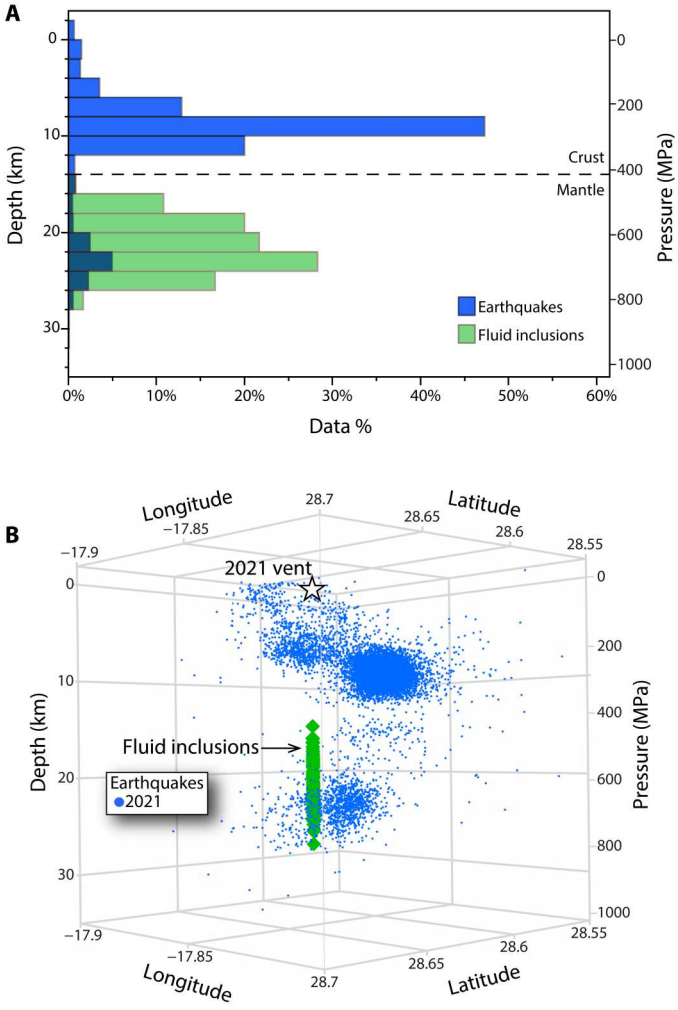

Fig. 3. Deep magma storage. (**A**) FI data fits in the deep seismic zone between ~20 and 25 km (*28*), indicating a zone of melt and crystal storage exhumed during eruption. (**B**) Three-dimensional comparison of the 2021 (syn-eruptive) earthquakes with our new FI depths from Raman CO_2 densities.

the 1949 eruption (*29*), reversely zoned olivine crystals are common within the first half of the 2021 eruption, indicating mantle replenishment and mixing with a more primitive liquid. Crystals from the second half of the eruption (LM0 and LM2) have uniform Mg# (82 to 86), and reverse-zoned crystals became less common. We found a general increase in the CO_2 densities and olivine Mg# as the eruption progressed (Fig. 2E), suggesting that crystals from deeper in the plumbing system were progressively transported upward as the eruption evolved and vacated the chamber.

We envision a scenario where the most primitive melt ascended from a deeper storage zone via dikes that cut the rigid lithospheric mantle (causing deep earthquakes at ~30 km), which has been proposed for previous eruptions along the CVR (*29*, *40*). This ascending melt then entered the main deep reservoir (~15 to 27 km) where olivine crystalized in the presence of a CO_2-rich fluid, trapping FI that recorded the pressure and depth location of this chamber. Alternatively, FI hosted in olivine may have crystallized at a deeper location (e.g., lithosphere-asthenosphere boundary) and re-equilibrated their densities at this level. From this main staging reservoir, geochemically primitive melts continued to ascend and mix with more evolved liquids at shallower levels before reaching the surface. This implies that olivine crystals and FI were either trapped or re-equilibrated in the magma reservoir between 15 and 27 km, before final ascent, mixing, and transport via a more evolved melt as also observed in other ocean islands (*1*, *25*, *39*–*43*).

To better elucidate the plumbing system under the CVR, we combined our new FI data with data from previous FI studies of La Palma (Fig. 4) (*39*). FI densities were converted to depths using the same procedure as described (Supplementary Materials). Most FI data come from minerals (clinopyroxene, plagioclase, apatite, amphibole, and olivine) within xenoliths, with more limited representation of phenocrysts (clinopyroxene and olivine). The FI data from xenoliths record depths of ~4 to 17 km, centered at ~10 km within the crust, with only the olivine grains within these xenolith populations reaching mantle depths (Fig. 4). FI in clinopyroxene phenocrysts record much shallower depths than olivine phenocrysts, mostly within the crust (average of ~12 km). This bimodal behavior among the phenocrysts is likely controlled by the well-developed cleavage in clinopyroxene that aids in their CO_2 re-equilibration during crustal storage (*12*), whereas olivine behaves as a more robust pressure vessel preserving mantle depths.

Notably, our FI-derived average depths are similar to those from olivine phenocryst hosted CO_2 FI from the eruption of 1949 (Fig. 4) (*1*, *29*). The 1949 density values of 0.85 to 0.89 g/cm^3 (versus our 0.73 to 0.98 g/cm^3) (*29*) correspond to pressures of 600 to 680 MPa (versus our 420 to 780 MPa). The wider range of pressures recorded by our primary FI potentially suggests a plumbing system with a more vertically extensive magma reservoir than the one recorded in 1949 (Fig. 4). The 1949 eruption was significantly smaller in magnitude (VEI 2) and only lasted 37 days (*29*), which could lead to the overlapping but smaller range of densities.

Our high-precision FI densities in olivine crystals document pressures constrained to a seismically active deep reservoir, indicating a unified location for olivine-bearing magma staging. While multiple magma reservoirs for the La Palma plumbing system have been recorded by different barometers and FI in other mineral phases (*1*, *25*), they do not reflect the main deep reservoir feeding the 2021 eruption, which was precisely (and rapidly) constrained using Raman-based FI barometry.

MATERIALS AND METHODS

Seven tephra samples were collected from a stratigraphic section of the 2021 eruption in January 2022 in the town of Las Manchas. Four samples were selected for FI study spanning the duration of the eruption. Olivine crystals covered with glass were handpicked under a stereoscope and cleaned in HBF_4 to dissolve glass coating. Single olivine crystals were then individually polished to identify primary FI, which were then photographed and analyzed using the WiTec Alpha300R Raman spectroscopy system in the Department of Earth and Atmospheric Sciences at Cornell University. Olivine and glass major element chemistry was obtained via the Cameca SX5-Tactis Electron Microprobe at the American Museum of Natural History in New York City. See all details in the Supplementary Materials.

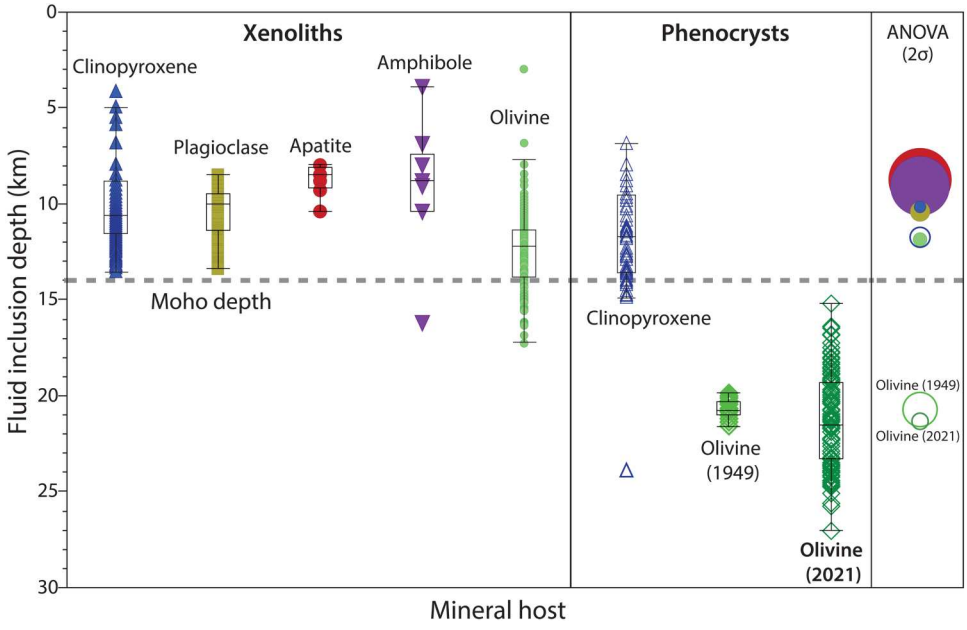

Fig. 4. Comparison of our new FI results (olivine 2021) with published FI data from Cumbre Vieja (*39*). Notice that the xenoliths and clinopyroxene phenocrysts record shallower levels of magma storage (within the crust) compared to olivine phenocrysts from the 1949 and 2021 eruptions, which preserve mantle depths. The circles on the right-hand side of the graph denote the result of analysis of variance (ANOVA) using Student's *t* test at the 95% confidence interval (2σ) to compare mean depth for each FI population. Open circles represent FI data from phenocrysts. FI densities converted to depths using the same treatment as reported for fig. S3.

Supplementary Materials

This PDF file includes:
Supplementary Text
Figs. S1 to S12
Tables S1 and S2
Data S2
References

Other Supplementary Material for this manuscript includes the following:
Data S1

REFERENCES AND NOTES

1. T. H. Hansteen, A. Klügel, H.-U. Schmincke, Multi-stage magma ascent beneath the Canary Islands: Evidence from fluid inclusions. *Contrib. Mineral. Petrol.* **132**, 48–64 (1998).
2. K. D. Putirka, Thermometers and barometers for volcanic systems. *Rev. Mineral. Geochem.* **69**, 61–120 (2008).
3. A. Nercessian, A. Hirn, J.-C. Lépine, M. Sapin, Internal structure of Piton de la Fournaise volcano from seismic wave propagation and earthquake distribution. *J. Volcanol. Geotherm. Res.* **70**, 123–143 (1996).
4. B. G. Ofeigsson, A. Hooper, F. Sigmundsson, E. Sturkell, R. Grapenthin, Deep magma storage at Hekla volcano, Iceland, revealed by InSAR time series analysis. *J. Geophys. Res.* **116**, (2011).
5. A. Klügel, S. Day, M. Schmid, B. Faria, Magma plumbing during the 2014–2015 eruption of Fogo (Cape Verde Islands). *Front. Earth Sci.* **8**, (2020).
6. X. Cui, Z. Li, H. Huang, Subdivision of seismicity beneath the summit region of Kilauea Volcano: Implications for the preparation process of the 2018 eruption. *Geophys. Res. Lett.* **48**, e2021GL094698 (2021).
7. D. C. Roman, K. V. Cashman, Top–down precursory volcanic seismicity: Implications for 'Stealth' magma ascent and long-term eruption forecasting. *Front. Earth Sci.* **6**, (2018).
8. R. Span, W. Wagner, A new equation of state for carbon dioxide covering the fluid region from the triple-point temperature to 1100 K at pressures up to 800 MPa. *J. Phys. Chem. Ref. Data Monogr.* **25**, 1509 (1996).
9. K. D. Putirka, H. Mikaelian, F. Ryerson, H. Shaw, New clinopyroxene-liquid thermobarometers for mafic, evolved, and volatile-bearing lava compositions, with applications to lavas from Tibet and the Snake River Plain, Idaho. *Am. Min.* **88**, 1542–1554 (2003).
10. D. A. Neave, K. D. Putirka, A new clinopyroxene-liquid barometer, and implications for magma storage pressures under Icelandic rift zones. *Am. Mineral.* **102**, 777–794 (2017).
11. A. Klügel, K. Galipp, K. Hoernle, F. Hauff, S. Groom, Geochemical and volcanological evolution of La Palma, Canary Islands. *J. Petrol.* **58**, 1227–1248 (2017).
12. T. H. Hansteen, A. Klugel, Fluid inclusion thermobarometry as a tracer for magmatic processes. *Rev. Mineral. Geochem.* **69**, 143–177 (2008).
13. C. Gansecki, R. L. Lee, T. Shea, S. P. Lundblad, K. Hon, C. Parcheta, The tangled tale of Kīlauea's 2018 eruption as told by geochemical monitoring. *Science* **366**, eaaz0147 (2019).
14. J. C. Carracedo, E. R. Badiola, H. Guillou, J. de La Nuez, F. J. Perez Torrado, Geology and volcanology of la Palma and El Hierro, Western Canaries. *Estud. Geol.* **57**, 175–273 (2001).
15. J. C. Carracedo, H. Guillou, S. Nomade, E. Rodriguez-Badiola, F. J. Perez-Torrado, A. Rodriguez-Gonzalez, R. Paris, V. R. Troll, S. Wiesmaier, A. Delcamp, J. L. Fernandez-Turiel, Evolution of ocean-island rifts: The northeast rift zone of Tenerife, Canary Islands. *Geol. Soc. Am. Bull.* **123**, 562–584 (2011).
16. M.-A. Longpré, Reactivation of Cumbre Vieja volcano. *Science* **374**, 1197–1198 (2021).
17. J. Fernandez, J. Escayo, A. G. Camacho, M. Palano, J. F. Prieto, Z. Hu, S. V. Samsonov, K. F. Tiampo, E. Ancochea, Shallow magmatic intrusion evolution below La Palma before and during the 2021 eruption. *Sci. Rep.* **12**, 20257 (2022).
18. J. C. Carracedo, V. R. Troll, J. M. D. Day, H. Geiger, M. Aulinas, V. Soler, F. M. Deegan, F. J. Perez-Torrado, G. Gisbert, E. Gazel, A. Rodriguez-Gonzalez, H. Albert, The 2021 eruption of the Cumbre Vieja volcanic ridge on La Palma Canary Islands. *Geol. Today* **38**, 94–107 (2022).
19. P. A. Torres-González, N. Luengo-Oroz, H. Lamolda, W. D'Alessandro, H. Albert, I. Iribarren, D. Moure-García, V. Soler, Unrest signals after 46 years of quiescence at Cumbre Vieja, La Palma, Canary Islands. *J. Volcanol. Geotherm. Res.* **392**, 106757 (2020).
20. J. Fernandez, J. Escayo, Z. Hu, A. G. Camacho, S. V. Samsonov, J. F. Prieto, K. F. Tiampo, M. Palano, J. J. Mallorqui, E. Ancochea, Detection of volcanic unrest onset in La Palma, Canary Islands, evolution and implications. *Sci. Rep.* **11**, 2540 (2021).
21. C. Bonadonna, M. Pistolesi, S. Biass, M. Voloschina, J. Romero, D. Coppola, A. Folch, L. D'Auria, A. Martin-Lorenzo, L. Dominguez, C. Pastore, M. P. Reyes Hardy, F. Rodríguez, Physical characterization of long-lasting hybrid eruptions: The 2021 Tajogaite eruption of Cumbre Vieja (La Palma, Canary Islands). *J. Geophys. Res.* **127**, e2022JB025302 (2022).

22. E. Roedder, in *Fluid Inclusions*, P. H. Ribbe, Ed. (Reviews in Mineralogy, Mineralogical Society of America, 1984), vol. 12, p. 644.
23. C. L. DeVitre, C. M. Allison, E. Gazel, A high-precision CO2 densimeter for Raman spectroscopy using a fluid density calibration apparatus. *Chem. Geol.* **584**, 120522 (2021).
24. I. H. Bell, J. Wronski, S. Quoilin, V. Lemort, Pure and pseudo-pure fluid thermophysical property evaluation and the open-source thermophysical property library CoolProp. *Ind. Eng. Chem. Res.* **53**, 2498–2508 (2014).
25. A. Klügel, T. H. Hansteen, K. Galipp, Magma storage and underplating beneath Cumbre Vieja volcano, La Palma (Canary Islands). *Earth Planet. Sci. Lett.* **236**, 211–226 (2005).
26. R. Tenzer, M. Bagherbandi, P. Vajda, Global model of the upper mantle lateral density structure based on combining seismic and isostatic models. *Geosci. J.* **17**, 65–73 (2013).
27. C. R. Ranero, M. Torne, E. Banda, Gravity and multichannel seismic reflection constraints on the lithospheric structure of the Canary Swell. *Mar. Geophys. Res.* **17**, 519–534 (1995).
28. L. D'Auria, I. Koulakov, J. Prudencio, I. Cabrera-Pérez, J. M. Ibánez, J. Barrancos, R. García-Hernández, D. Martínez van Dorth, G. D. Padilla, M. Przeor, V. Ortega, P. Hernández, N. M. Peréz, Rapid magma ascent beneath La Palma revealed by seismic tomography. *Sci. Rep.* **12**, 17654 (2022).
29. A. Klügel, H. U. Schmincke, J. D. L. White, K. A. Hoernle, Chronology and volcanology of the 1949 multi-vent rift-zone eruption on La Palma (Canary Islands). *J. Volcanol. Geotherm. Res.* **94**, 267–282 (1999).
30. K. Galipp, A. Klügel, T. H. Hansteen, Changing depths of magma fractionation and stagnation during the evolution of an oceanic island volcano: La Palma (Canary Islands). *J. Volcanol. Geotherm. Res.* **155**, 285–306 (2006).
31. A. K. Barker, V. R. Troll, J. C. Carracedo, P. A. Nicholls, The magma plumbing system for the 1971 Teneguía eruption on La Palma, Canary Islands. *Contrib. Mineral. Petrol.* **170**, (2015).
32. J. M. Castro, Y. Feisel, Eruption of ultralow-viscosity basanite magma at Cumbre Vieja, La Palma, Canary Islands. *Nat. Commun.* **13**, 3174 (2022).
33. P. E. Wieser, A. J. F. Kent, C. B. Till, J. Donovan, D. A. Neave, D. L. Blatter, M. J. Krawczynski, Barometers behaving badly: Assessing the influence of analytical and experimental uncertainty on clinopyroxene thermobarometry calculations at crustal conditions. *J. Petrol.* , egac126 (2022).
34. R. J. Bodnar, Reequilibration of fluid inclusions, in *Fluid Inclusions: Analysis and Interpretation*, I. Samson, A. Anderson, D. Marshall, Eds. (Short Course 32, Mineralogical Association of Canada, 2003), pp. 213–230.
35. M. Campione, Threshold effects for the decrepitation and stretching of fluid inclusions. *J. Geophys. Res. Solid Earth* **123**, 3539–3548 (2018).
36. B. J. Wanamaker, T.-F. Wong, B. Evans, Decrepitation and crack healing of fluid inclusions in San Carlos olivine. *J. Geophys. Res. Solid Earth* **95**, 15623–15641 (1990).
37. M. Campione, N. Malaspina, M. L. Frezzotti, Threshold size for fluid inclusion decrepitation. *J. Geophys. Res. Solid Earth* **120**, 7396–7402 (2015).
38. B. J. Wanamaker, B. Evans, Mechanical re-equilibration of fluid inclusions in San Carlos olivine by power-law creep. *Contrib. Mineral. Petrol.* **102**, 102–111 (1989).
39. A. Klügel, M.-A. Longpré, L. García-Cañada, J. Stix, Deep intrusions, lateral magma transport and related uplift at ocean island volcanoes. *Earth Planet. Sci. Lett.* **431**, 140–149 (2015).
40. A. Klügel, E. Albers, T. H. Hansteen, Mantle and crustal xenoliths in a tephriphonolite from La Palma (Canary Islands): Implications for phonolite formation at Oceanic Island volcanoes. *Front. Earth Sci.* **10**, 761902 (2022).
41. M. L. Frezzotti, J. L. R. Touret, W. J. Lustenhouwer, E.-R. Neumann, Melt and fluid inclusions in dunite xenoliths from La Gomera, Canary Islands: Tracking the mantle metasomatic fluids. *Eur. J. Mineral.* **6**, 805–818 (1994).
42. M. L. Frezzotti, T. Anderson, E.-R. Neumann, S. L. Simonsen, Carbonatite melt–CO2 fluid inclusions in mantle xenoliths from Tenerife, Canary Islands: A story of trapping, immiscibility and fluid–rock interaction in the upper mantle. *Lithos* **64**, 77–96 (2002).
43. E.-R. Neumann, W. Wulff-Pedersen, L. Johnsen, T. Andersen, E. Krogh, Petrogenesis of spinel harzburgite and dunite suite xenoliths from Lanzarote, eastern Canary Islands: Implications for the upper mantle. *Lithos* **35**, 83–107 (1995).
44. J. E. Romero, M. Burton, F. Cáceres, J. Taddeucci, R. Civico, T. Ricci, M. J. Pankhurst, P. A. Hernández, C. Bonadonna, E. W. Llewellin, M. Pistolesi, M. Polacci, C. Solana, L. D'Auria, F. Arzilli, D. Andronico, F. Rodríguez, M. Asensio-Ramos, A. Martín-Lorenzo, C. Hayer, P. Scarlato, N. M. Perez, The initial phase of the 2021 Cumbre Vieja ridge eruption (Canary Islands): Products and dynamics controlling edifice growth and collapse. *J. Volcanol. Geotherm. Res.* **431**, 107642 (2022).
45. J. M. D. Day, V. R. Troll, M. Aulinas, F. M. Deegan, H. Geiger, J. C. Carracedo, G. G. Pinto, F. J. Perez-Torrado, Mantle source characteristics and magmatic processes during the 2021 La Palma eruption. *Earth Planet. Sci. Lett.* **597**, 117793 (2022).
46. K. Dayton, G. Gazel, P. Wieser, Deep magma storage during the 2021 La Palma eruption. *Zenodo*, https://doi.org/10.5281/zenodo.7510719, (2023).
47. F. Lin, R. J. Bodnar, S. P. Becker, Experimental determination of the Raman CH4 symmetric stretching (ν1) band position from 1–650bar and 0.3–22°C: Application to fluid inclusion studies. *Geochim. Cosmochim. Acta* **71**, 3746–3756 (2007).
48. X. Wang, I. M. Chou, W. Hu, R. C. Burruss, Q. Sun, Y. Song, Raman spectroscopic measurements of CO2 density: Experimental calibration with high-pressure optical cell (HPOC) and fused silica capillary capsule (FSCC) with application to fluid inclusion observations. *Geochim. Cosmochim. Acta* **75**, 4080–4093 (2011).
49. H. M. Lamadrid, L. R. Moore, D. Moncada, J. D. Rimstidt, R. C. Burruss, R. J. Bodnar, Reassessment of the raman CO_2 densimeter. *Chem. Geol.* **450**, 210–222 (2017).
50. R. J. Bakker, Package FLUIDS 1. Computer programs for analysis of fluid inclusion data and for modelling bulk fluid properties. *Chem. Geol.* **194**, 3–23 (2003).
51. D. M. Sublett, E. Sendula, H. M. Lamadrid, M. Steele-MacInnis, G. Spiekermann, R. J. Bodnar, Raman spectral behavior of N_2, CO_2, and CH_4 in N_2–CO_2–CH_4 gas mixtures from 22°C to 200°C and 10 to 500 bars, with application to other gas mixtures. *J. Raman Spectrosc.* **52**, 750–769 (2021).
52. K. P. Jochum, U. Weis, B. Schwager, B. Stoll, S. A. Wilson, G. H. Haug, M. O. Andreae, J. Enzweiler, Reference values following ISO guidelines for frequently requested rock reference materials. *Geostand. Geoanal. Res.* **40**, 333–350 (2016).
53. E. Jarosewich, J. A. Nelen, J. A. Norberg, Reference samples for electron microprobe analysis. *Geostand. Newsl.* **4**, 43–47 (1980).
54. National Geographic Institute (IGN), Spanish Seismic Catalog (2022); https://doi.org/10.7419/162.03.2022.
55. B. R. Lienert, J. Havskov, A computer program for locating earthquakes both locally and globally. *Seismol. Res. Lett.* **66**, 26–36 (1995).
56. J. Havskov, L. Ottemöller, SeisAn earthquake analysis software. *Seismol. Res. Lett.* **70**, 532–534 (1999).
57. J. J. Rueda Núñez, R. Abella Meléndez, M. J. Blanco Sánchez, E. A. Díaz Suárez, I. F. Domínguez Cerdeña, J. Domínguez Valbuena, M. Fernández de Villalta Compagni, C. del Fresno Rodríguez-Portugal, R. L. López Díaz, C. López Moreno, M. López Muga, A. Muñoz Santamaría, *Revisión del Catálogo Sísmico de las Islas Canarias (1341–2000)* (Instituto Geográfico Nacional, 2020).
58. T. Walter, T. Dahm, S. Cesca, C. Valenzuela Malebran, C. Milkereit, N. Richter, A. Shevshenko, D. Vollmer, M. Kriegerowski, HART-La Palma volcanic eruption (2021). 10.14470/4N7576350874.
59. P. Lesage, M. J. Heap, A. Kushnir, A generic model for the shallow velocity structure of volcanoes. *J. Volcanol. Geotherm. Res.* **356**, 114–126 (2018).
60. S. M. Sterner, K. S. Pitzer, An equation of state for carbon dioxide valid from zero to extreme pressures. *Contrib. Mineral. Petrol.* **117**, 362–374 (1994).
61. M. Petrelli, L. Caricchi, D. Perugini, Machine learning thermo-barometry: Application to clinopyroxene-bearing magmas. *J. Geophys. Res. Solid Earth* **125**, e2020JB020130 (2020).
62. P. E. Wieser, M. Petrelli, J. Lubbers, E. Wieser, S. Özaydin, A. J. F. Kent, C. B. Till, Thermobar: An open-source Python3 tool for thermobarometry and hygrometry. *Volcanica* **5**, 349–384 (2022).
63. R. L. Roeder, R. F. Emslie, Olivine-liquid equilibrium. *Contrib. Mineral. Petrol.* **29**, 275–289 (1970).
64. M. J. Toplis, The thermodynamics of iron and magnesium partitioning between olivine and liquid: Criteria for assessing and predicting equilibrium in natural and experimental systems. *Contrib. Mineral. Petrol.* **149**, 22–39 (2005).
65. Y. Moussallam, M.-A. Longpré, C. McCammon, A. Gomez-Ulla, E. F. Rose-Koga, B. Scaillet, N. Peters, E. Gennaro, R. Paris, C. Oppenheimer, Mantle plumes are oxidised. *Earth Planet. Sci. Lett.* **527**, 115798 (2019).
66. K. Putirka, M. Johnson, R. Kinzler, J. Longhi, D. Walker, Thermobarometry of mafic igneous rocks based on clinopyroxene-liquid equilibria, 0–30 kbar. *Contrib. Mineral. Petrol.* **123**, 92–108 (1996).

Acknowledgments: We thank S. Bergen for sample processing, C. DeVitre for data assistance, and K. Hammond and N. Tailby at AMNH for EPMA assistance. We are grateful to PEVOLCA for enabling access to the Exclusion Zone of La Palma during the 2021 eruption for sample collection. D.C.R. thanks L. D'Auria and I. Koulakov for assistance and guidance regarding La Palma earthquake locations and seismic data. **Funding:** This work was supported by NASA Interdisciplinary Science grant 80NSSC20K1674 (to E.G.); National Science Foundation grants EAR 1826673 (to E.G.), 2216738 (to E.G.), and 2217371 (to P.W.); LAJIAL (PGC2018-101027-B-I00, MCIU/AEI/FEDER, EU); and MESVOL (SD RD 1078/2021 LA PALMA). **Author contributions:** Conceptualization: E.G., P.W., and K.D. Data curation: K.D. Formal analysis: K.D., E.G., and P.W. Funding acquisition: E.G. Investigation: E.G., K.D., J.W., H.L.M., and D.C.R. Methodology: K.D., E.G., and P.W. Resources: E.G., V.R.T., and J.C.C. Software: P.W. Supervision: E.G. Visualization: K.D., E.G., and P.W. Writing—original draft: E.G. and K.D. Writing—review and editing: K.D., E.G., P.W., V.R.T., J.C.C., M.A., H.G., F.M.D., G.G., F.J.P.-T., and D.C.R. **Competing interests:** The authors declare that they have no competing interests. **Data and materials availability:** All data needed to

evaluate the conclusions in the paper are present in the paper and/or the Supplementary Materials. All produced data are contained in data S1, with raw data and python scripts deposited at https://doi.org/10.5281/zenodo.7510719 (data S2) (*46*).

Submitted 6 September 2022
Accepted 9 January 2023
Published 8 February 2023
10.1126/sciadv.ade7641